Design optimization of high breakdown voltage vertical GaN junction barrier Schottky diode with high-K/low-K compound dielectric structure

Kuiyuan Tian(田魁元), Yong Liu(刘勇), Jiangfeng Du(杜江锋)[†], and Qi Yu(于奇)

State Key Laboratory of Electronic Thin Films and Integrated Devices, University of Electronic Science and Technology of China, Chengdu 610054, *China*

(Received 24 June 2022; revised manuscript received 19 August 2022; accepted manuscript online 2 September 2022)

A vertical junction barrier Schottky diode with a high-K/low-K compound dielectric structure is proposed and optimized to achieve a high breakdown voltage (BV). There is a discontinuity of the electric field at the interface of high-K and low-K layers due to the different dielectric constants of high-K and low-K dielectric layers. A new electric field peak is introduced in the n-type drift region of junction barrier Schottky diode (JBS), so the distribution of electric field in JBS becomes more uniform. At the same time, the effect of electric-power line concentration at the p–n junction interface is suppressed due to the effects of the high-K dielectric layer and an enhancement of breakdown voltage can be achieved. Numerical simulations demonstrate that GaN JBS with a specific on-resistance ($R_{on,sp}$) of 2.07 mΩ·cm^2 and a BV of 4171 V which is 167% higher than the breakdown voltage of the common structure, resulting in a high figure-of-merit (FOM) of 8.6 GW/cm^2, and a low turn-on voltage of 0.6 V.

Keywords: GaN junction barrier Schottky diode, compound dielectric, breakdown voltage, turn-on voltage

PACS: 73.61.Ey, 73.40.Kp, 77.22.Ch, 85.30.Mn **DOI:** 10.1088/1674-1056/ac8e99

1. Introduction

Gallium nitride (GaN) materials are very suitable for fabricating high-power devices due to wide band gap, high saturation electron mobility, high critical breakdown field, good thermal conductivity, and superior Baliga's figure-of-merit than SiC and Si.[1–4] Recently, the demonstration of low leakage current and high breakdown voltage (BV) vertical GaN diodes has become a major focus in the field of power electronics.[5–8] However, the high turn-on voltage ($V_{on} > 3$ V) will cause a high conduction loss in power switching applications in p–n junction diodes.[9–11] And for vertical GaN Schottky barrier diodes (SBDs), there is an electric field peak at the Schottky contact, which can lead to a high tunneling current of the Schottky barrier.[12,13] In the past few years, vertical GaN JBS diodes have been fabricated by forming p–n junction on the basis of vertical GaN SBDs.[14,15] The JBS can reduce the leakage current of high voltage operation without sacrificing the positive characteristics, because a thick barrier produced by the p–n junction is only added to the high electric field region, and the tunneling current can be reduced significantly. However, the electric field of the p–n junction is not uniform enough in GaN JBS and causes premature breakdown, thus hindering the improvement of BV of JBS with low leakage current.

Some literature has reported the structure of a high-K dielectric layer as a passivation layer.[16–18] The structure can improve the reverse breakdown voltage of the device effectively by utilizing the characteristic that the electric field distribution in the high-K dielectric layer tends to be uniform. When the high-K dielectric layer is used as a passivation layer of a semiconductor device, the electric field distribution inside the device is modulated and tends to be uniform, so the BV of the device is increased. However, the use of only high-K dielectric layers is far from the theoretical limit of GaN reverse characteristics. By utilizing a composite dielectric structure composed of a high-K dielectric layer and a low-K dielectric layer, we have reported a GaN p–n junction diode having high reverse characteristics.[19]

In this paper, a vertical GaN-based JBS with a high-K/low-K compound dielectric structure (GaN VCD-JBS) is proposed to increase the breakdown voltage of conventional JBS and reduce the effects of electric field crowding at the tip of the p–n junction without sacrificing forward characteristic. The breakdown voltage of the proposed GaN VCD-JBS is improved by optimizing the parameters of the device. Then, the highest figure-of-merit of 8.6 GW/cm^2 is obtained in comparison with the papers recently reported.

2. Device structure

The device structure of the proposed GaN VCD-JBS is shown in the following Fig. 1. The simulated epitaxial GaN structure consists of a 15-μm-thick GaN drift region doped with 1×10^{16} cm^{-3}, which acts as a current path and pressure-resistant structure. Then two p-type regions doped with 1×10^{18} cm^{-3} are formed. The depth and length of the p-type region are 1 μm and 2 μm, respectively. Two Si_3N_4

[†]Corresponding author. E-mail: jfdu@uestc.edu.cn

© 2023 Chinese Physical Society and IOP Publishing Ltd

high-K dielectric layers are added to both sides of GaN JBS while two SiO_2 low-K dielectric layers are placed at the bottom of the high-K layers mentioned above. The device has a length (L_{JBS}) of 5.5 μm and a thickness (T_{JBS}) of 15 μm, respectively. For convenience, the width of Schottky contact, the distance from the interface of the p–n junction in JBS to the SiO_2 low-K dielectric layer, and the length of the dielectric layer are labeled as W_n, T, and L respectively.

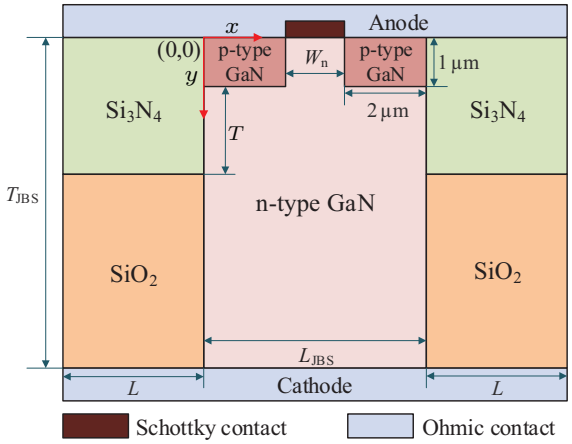


Fig. 1. Schematic cross-section of GaN VCD-JBS.

According to Gauss's law and Poisson's equation, when the electric fluxes are equal at the interface of two materials with different dielectric constants, the electric field strength along the direction of the electric displacement vector inside the two materials satisfies the following relationship:

$$\varepsilon_{\text{high } K} \cdot E_{\text{high } K} = \varepsilon_{\text{low } K} \cdot E_{\text{low } K}. \tag{1}$$

Since the dielectric constant of Si_3N_4 is 7.5 and the dielectric constant of SiO_2 is 3.9, it can be seen from the formula that the electric field at the interface of the Si_3N_4 material layer and the SiO_2 material layer is discontinuous. The electric field in the vertical direction has a lift from the Si_3N_4 material layer to the SiO_2 material layer. Based on this principle, we designed a GaN VCD-JBS with a high breakdown voltage. JBS depends on the p–n junction formed by the p-type doping region and the n-type drift region which generates a depletion region in n-type GaN to withstand voltage without increasing turn-on voltage. However, the electric field away from the p–n junction interface in the n-type GaN is drastically reduced, which leads to a reduction in breakdown voltage. In this work, we use the discontinuous electric field in the dielectric layer to affect the electric field in the n-type GaN. By increasing the electric field in the n-type GaN away from the p–n junction interface, the electric field in the n-type drift region becomes uniform, so that the breakdown voltage is increased without sacrificing forward characteristics such as specific on-resistance, saturation current, and turn-on voltage. Then, by optimizing the vertical high-K/low-K compound dielectric structure and balancing the size of the Schottky contact area, the electric field away from the p–n junction is more uniform keeping the doping concentration constant.

3. Simulation models and calibration

3.1. Simulation models

In the process of simulation, low-field mobility model, high-field mobility model, Shockley–Read–Hall (SRH) model, Fermi–Dirac model, Auger model, bandgap narrowing model, phonon-assisted tunneling model for GaN SBD, and the Selberherr's impact ionization model are adopted. The reverse I–V characteristics of GaN diodes can be well explained by the phonon-assisted tunneling model.[20] The tunneling current is generated by the emission of electrons from the energy level of the metal–semiconductor interface. The density of the tunneling current is

$$J = qN_sW. \tag{2}$$

In which q describes the electron charge, N_s describes the occupied density of states at the interface, and W is the phonon-assisted tunneling rate as a function of temperature T and electric field strength E:

$$W = \frac{qE}{(8m^*\varepsilon_T)} \frac{\sqrt{(1+\gamma^2)^{1/2}-\gamma}}{(1+\gamma^2)^{1/4}} \times \exp\left(-\frac{4}{3}\frac{\sqrt{2m^*}}{qE\hbar}\varepsilon_T^{3/2}\left(\sqrt{1+\gamma^2}-\gamma\right)^2 \times \left(\sqrt{1+\gamma^2}+\frac{1}{2}\gamma\right)\right), \tag{3}$$

$$\gamma = \frac{\sqrt{2m^*}\Gamma^2}{8qE\hbar\varepsilon_T^{1/2}}. \tag{4}$$

Here Γ^2 is the width of the central absorption band

$$\Gamma^2 = 8a(\hbar\omega)^2\left(\frac{2}{\exp(\hbar\omega/k_BT)-1}+1\right), \tag{5}$$

where a describes the electron–phonon interaction constant, $\hbar\omega$ describes the phonon energy, and ε_T describes the trap depth.

In this paper, low-field mobility and high-field mobility models are used as carrier mobility models. The Albrecht model is selected as low-field mobility for simulation, and the low-field mobility of carriers is described as

$$\frac{1}{\mu(N,T)} = \frac{a\cdot N}{N_0}\left(\frac{T}{T_0}\right)^{-3/2}\ln\left(1+3\left(\frac{T}{T_0}\right)^2\left(\frac{N}{N_0}\right)^{-2/3}\right) + b\left(\frac{T}{T_0}\right)^{3/2} + \frac{c}{\exp(T_1/T)-1}, \tag{6}$$

where $\mu(N,T)$ is the low-field carrier mobility as a function of doping concentration N and lattice temperature T, where a, b, c, T_0, N_0, and T_1 are obtained from Monte Carlo fitting results, The results are 2.61×10^{-4} V·s·cm^{-2}, 2.9×10^{-4} V·s·cm^{-2},

170.0×10^{-4} V·s·cm^{-2}, 300 K, 1.0×10^{-17} cm^{-3}, 1065 K, respectively.[21]

The high field mobility of charge carriers is described as

$$\mu(E)=\frac{\mu(N,T)+V_{\rm sat}[E^{(n_1-1)}/E_{\rm C}^{n_1}]}{1+\alpha(E/E_{\rm C})^{n_2}+(E/E_{\rm C})^{n_1}}, \tag{7}$$

where $\mu(E)$ is the high-field carrier mobility as a function of the electric field strength E, $V_{\rm sat}$, $E_{\rm C}$, α, n_1, and n_2 are obtained from the Monte Carlo fitting results, and the results are 1.9064×10^7 cm/s, 220.8936 kV/cm, 6.1973, 7.2044, 0.7857, respectively.[22]

In this paper, the impact ionization model is selected as Selberherr's impact ionization model, and the collision ionization rate of electrons ($\alpha_{\rm n}$) and holes ($\alpha_{\rm p}$) are respectively described as

$$\alpha_{\rm n}=a_{\rm n}\exp\left[-\left(\frac{b_{\rm n}}{E}\right)^m\right], \tag{8}$$

$$\alpha_{\rm p}=a_{\rm p}\exp\left[-\left(\frac{b_{\rm p}}{E}\right)^m\right], \tag{9}$$

where E is the local electric field, $a_{\rm n}$, $b_{\rm n}$, $a_{\rm p}$, $b_{\rm p}$, and m are obtained from Monte Carlo simulation results, which are 2.52×10^8 cm^{-1}, 3.41×10^7 V/cm, 5.37×10^6 cm^{-1}, 1.96×10^7 V/cm, 1, respectively.[23]

3.2. Simulation calibration

The GaN vertical p–n diode reported by Esmat Farzana has been used to calibrate the simulation model.[24] The reported diode is grown on a free-standing substrate with an epitaxial dislocation density of 10^6 cm^{-2}. The epitaxial structure consists of a 0.25-μm layer of n+GaN ([Si]: 1×10^{19} cm^{-3}), followed by a 4-μm layer of undoped GaN as the n-drift layer, a 0.4-μm layer of p+GaN ([Mg]: 3×10^{19} cm^{-3}) layers, and a 10-nm p++GaN ([Mg]: 3×10^{20} cm^{-3}) layer to make ohmic contacts. The GaN p–n diode was simulated by the Silvaco ATLAS tool and the above model was used to calibrate the simulation model parameters. The simulated GaN p–n diode has a turn-on voltage of 3 V and a breakdown voltage of 1100 V, which is similar to the experimental results. The forward characteristics and the electric field characteristics of the reported GaN vertical diodes and the simulation results are shown in Fig. 2. The simulation results show great fitting accuracy, proving the credibility of our model for the GaN vertical diode.

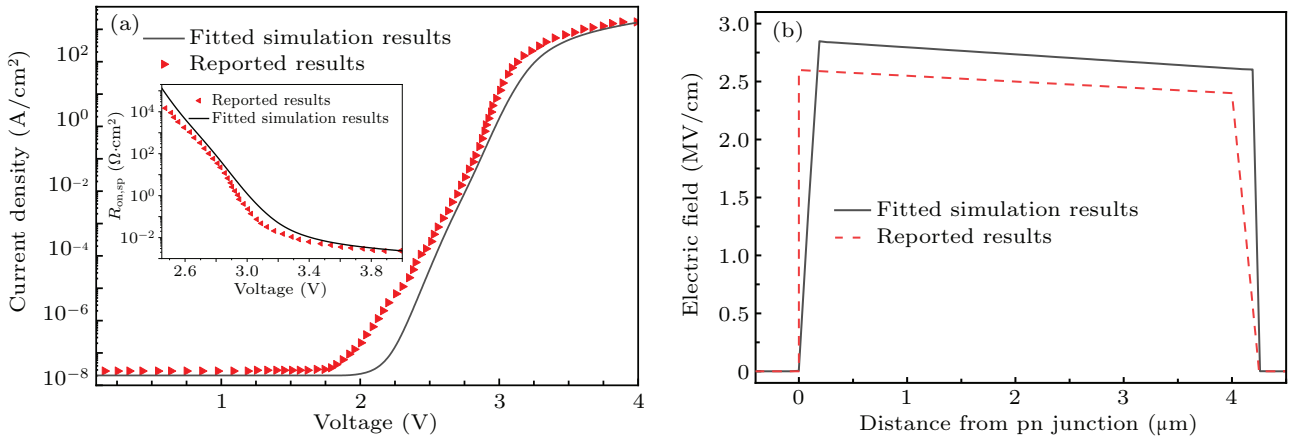


Fig. 2. (a) Comparison of the simulated and reported forward characteristics. (b) Comparison of simulated electric field and reported electric field in the diode drift region.

4. Results and discussion

Figure 3 shows the forward and reverse characteristics of the conventional GaN SBD, the conventional GaN JBS, the GaN JBS with SiO_2 dielectric layer, and the GaN VCD-JBS designed in the work. As shown in Fig. 3. The breakdown voltage of the conventional SBD is 320 V, while the breakdown voltage of the conventional JBS shown in Fig. 3 is 2262 V. The reason is that the p-type doping region implanted inside the JBS forms a p–n junction with the n-type drift region. In the case of withstanding voltage, the high electric field which should have been on the Schottky contact surface is transferred to the p–n junction inside the device. At the same time, the p–n junction forms a higher barrier than the Schottky barrier and can withstand higher voltages. For GaN VCD-JBS, the *BV* is 3165 V when the length of the dielectric layer $L=4$ μm and the distance from the p–n junction interface to the low-*K* dielectric layer $T=5$ μm, while the breakdown voltage of the GaN JBS with only SiO_2 dielectric layer is 2585 V. The results confirmed that the layer of high *K*/low *K* compound dielectric can effectively modulate the electric field and effectively improve the withstand voltage.

The inset of Fig. 3 shows a comparison of the output characteristics of conventional GaN SBD, conventional GaN JBS, GaN JBS with SiO_2 dielectric layer, and GaN VCD-JBS. Simulated results show that the turn-on voltage of GaN VCD-JBS is 0.6 V, which is comparable to conventional GaN-based SBD and conventional GaN-based JBS and much less than the turn-on voltage of the p–n diode (> 3 V). As can be seen from the

inset of Fig. 3, the forward current density of GaN VCD-JBS, GaN JBS with SiO_2 dielectric layer and conventional GaN JBS is slightly less than the forward current density of GaN SBD, because the Schottky contact area is reduced due to the presence of a p–n junction in the JBS. However, compared with p–n junction diodes of the same size, the forward characteristics are significantly improved.

Figure 4 shows the equipotential contours of the conventional GaN JBS, GaN JBS with SiO_2 dielectric layer, and designed GaN VCD-JBS. As shown in Fig. 4, the depletion depth of the drift region in conventional JBS is shorter than the depletion depth of the drift region in VCD GaN JBS. Meanwhile, the potential in the dielectric layers on both sides can also help to withstand voltage. Simulation results show that the n-type drift region can be increased significantly and a higher breakdown voltage can be achieved by optimizing the high-*K*/low-*K* dielectric layer.

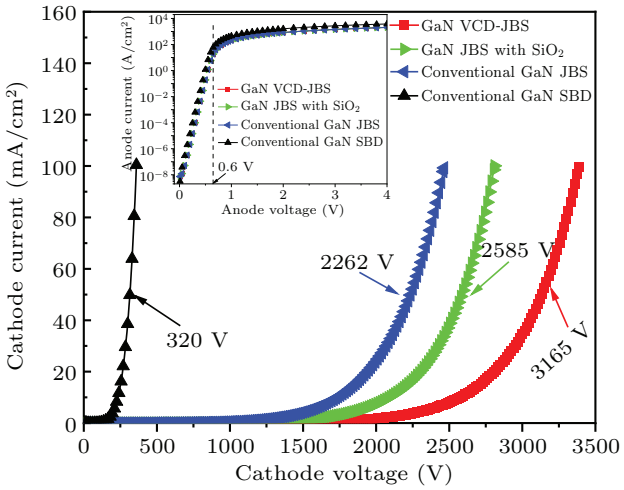


Fig. 3. Reverse *I*–*V* characteristics of the conventional GaN SBD, the conventional GaN JBS, the GaN JBS with SiO_2 dielectric layer, and the GaN VCD-JBS. The inset shows the forward *I*–*V* characteristics of the conventional GaN SBD, the conventional GaN JBS, the GaN JBS with SiO_2 dielectric layer, and the GaN VCD-JBS.

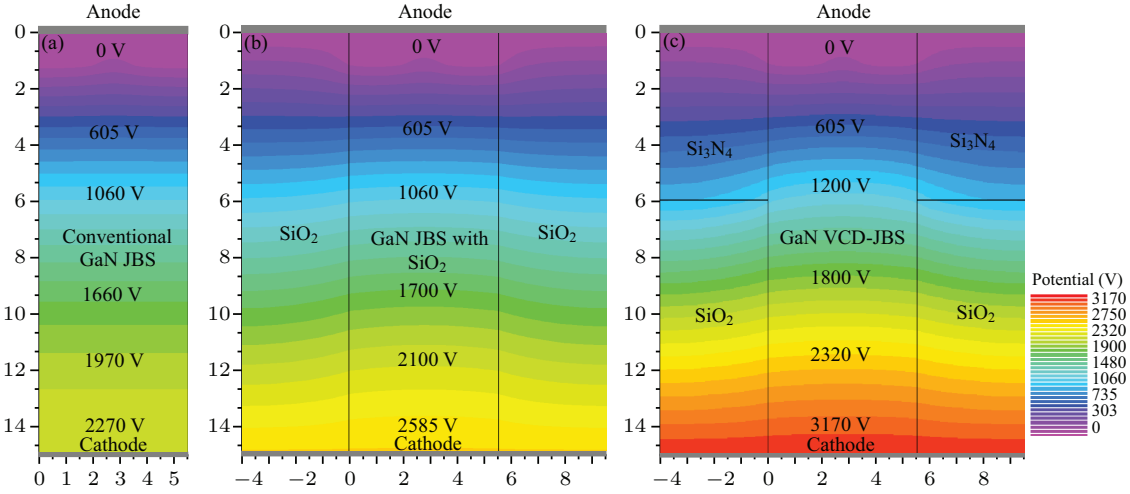


Fig. 4. Simulated equipotential contours when breakdown for (a) the conventional GaN JBS, (b) the GaN JBS with SiO_2 dielectric layer, and (c) the GaN VCD-JBS.

Figure 5 shows the electric field distribution of the conventional GaN JBS, the GaN JBS with SiO_2 dielectric layer, and GaN VCD-JBS when the dimension of the JBS is 15 μm and the electric field curve distribution of the two devices when $x = 0.1$ μm. As shown in Figs. 5(a) and 5(b), the electric field is concentrated on the p–n junction of JBS and decreases away from the interface of the p–n junction in the n-type drift region. As shown in Fig. 5(c), there is a discontinuity of electric field at the interface of Si_3N_4 and SiO_2 due to the different dielectric constants of Si_3N_4 and SiO_2. The electric field of Si_3N_4 at the interface is suppressed and the electric field of SiO_2 is enhanced.

As shown in Fig. 5(d), the areas enclosed by the electric field curves of conventional GaN JBS and GaN JBS with SiO_2 dielectric layer are approximately triangular, and the electric field gradually decreases as the distance from the p–n junction increases. As we all know, the integral of the electric field over the depletion region can represent the withstand voltage of the region. For GaN VCD-JBS, by introducing a high-*K*/low-*K* dielectric layer, the electric field in the drift region away from the p–n junction is increased, and the electric field distribution tends to be uniform. However, due to the electric field crowding effect, the electric field is concentrated at the sharp spike of the p–n junction interface. The peak electric field of the sharp spike is relatively high, so the electric field at other areas of the p–n junction interface is lower than the critical breakdown electric field when the device is breaking down. As shown in the inset of Fig. 5(d), the addition of a high-*K*/low-*K* dielectric layer is equivalent to the introduction of a high electric field at the contact surface of the dielectric layer and GaN JBS, which improves the electric field away from the spikes of the p–n junction interface, further increasing the breakdown voltage. Compared to a conventional junction termination, the proposed structure raises the electric fields in the n-type region away from the p–n junction interface.

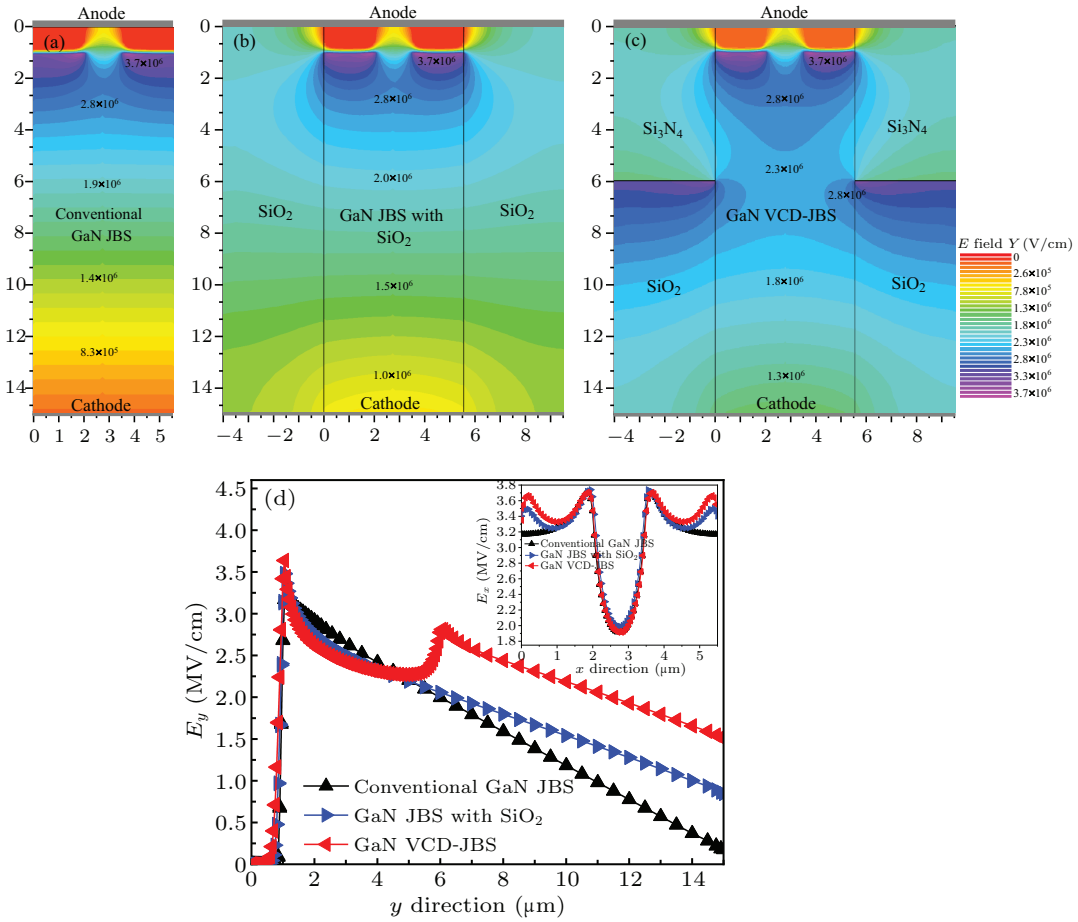


Fig. 5. The distribution of electric field for (a) the conventional GaN JBS, (b) the GaN JBS with SiO_2 dielectric layer, and (c) the GaN VCD-JBS. (d) The electric field profile at $x = 0.1$ μm. The inset of (d) shows the electric field profile at $y = 1$ μm.

We investigate the relationship between BV and the distance from the p–n junction interface to low-K dielectric layer T and the length of the dielectric layer L. For convenience of further investigation, GaN VCD-JBS with one block of low-K and one block of high-K on both sides is optimized firstly by Silvaco simulation. The distance between p–n junction and low-K dielectric layer varied from 1 μm to 11 μm, and the length of the dielectric layer was changed from 1 μm to 12 μm. When the leakage current is detected to be 50 mA/cm^2 in the Silvaco simulation, the voltage is defined as the breakdown voltage.

Figure 6 shows the relationship between the breakdown voltage and the length of the dielectric layer L. The inset of Fig. 6 shows the relationship between the breakdown voltage and the distance from the interface of p–n junction to the low K dielectric layer T. As the length of the dielectric layer L increases, the breakdown voltage gradually increases until saturation. When the length of the dielectric layer reaches 10 μm, the breakdown voltage of GaN VCD-JBS reaches the maximum value. However, longer dielectric layers result in a waste of conductive area in the device. The length of the dielectric layer $L = 4$ μm has been chosen, and the device has a large breakdown voltage with a small size. With the increase of T, the breakdown voltage increases firstly and then decreases. If the distance between the p–n junction interface and the low-K dielectric layer is undersized, a high electric field peak close to the p–n junction in JBS causes a premature breakdown. But if the distance between the p–n junction interface and the low-K dielectric layer is too large, the new electric field peak introduced in the n-type drift region is relatively low and causes a low breakdown voltage. The distance between the p–n junction interface and the low-K dielectric layer $T = 5$ μm has been chosen. When $T = 5$ μm, the breakdown voltage of GaN VCD-JBS reaches the maximum value.

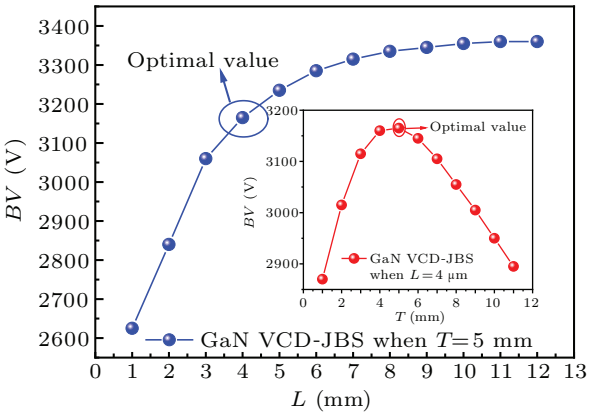


Fig. 6. Relationship between BV and L when $T = 5$ μm. The inset shows the relationship between BV and T when $L = 4$ μm.

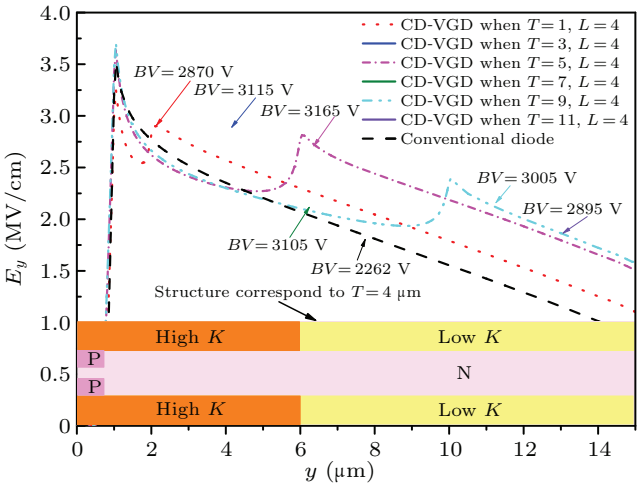


Fig. 7. Electric field distributions for various T at $x = 0.1$ μm when $L = 4$ μm.

Figure 7 shows that the electric field distribution inside the device varies with the variety of the distance between p–n junction interface and low-K dielectric layer T when it breaks down. The breakdown voltages of the device can be observed by the different electric field distributions inside the devices. With the observation of Fig. 7, the breakdown voltage of conventional GaN JBS is 2262 V. By optimizing the distance between interface of the p–n junction and the low-K dielectric layer T, the electric field in JBS becomes more uniform. When T is optimized to be 5 μm, the GaN VCD-JBS achieves a $BV = 3165$ V, which is larger by 38% than conventional GaN JBS.

For GaN JBS diodes, the Schottky contact area is important for the forward and reverse characteristics of the diode. As the width of the Schottky contact region increases, the specific on-resistance of the JBS ($R_{on,sp}$) will decrease. However, the wide Schottky contact increases the reverse leakage current of the diode and reduces the breakdown voltage.

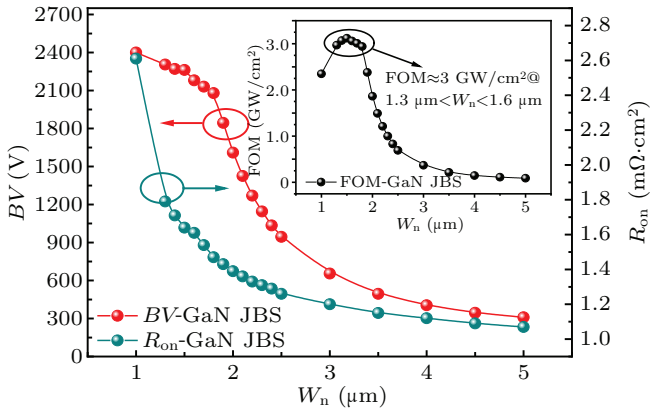


Fig. 8. BV and R_{on} as functions of the Schottky contact width of GaN conventional JBS W_n. The inset shows the figures-of-merit (F_{OM}) of GaN JBS.

Figure 8 shows the relationship between the BV and R_{on} and the Schottky contact width of GaN conventional JBS W_n obtained by simulation. As the Schottky contact width increases, the device's resistance gradually decreases, but the BV of the JBS diode also decreases. From the inset of Fig. 8, we can conclude that the figure-of-merit (F_{OM}) of JBS increases firstly and then decreases with W_n increasing. In the range of W_n between 1.3 μm and 1.6 μm, the F_{OM} of JBS reaches 3 GW/cm^2. Therefore, we choose 1.5 μm as the Schottky contact width of the device.

Figure 9 shows the electric field distribution of the two cells' combination of GaN VCD-JBS at the breakdown voltage. The optimized structure above is just one cell of a complete GaN VCD-JBS. The complete GaN VCD-JBS consists of many identical cells in parallel. A cell and the adjacent cell share a common dielectric layer. Therefore, it is necessary to verify whether the GaN VCD-JBS composed of two or more cells can achieve the effect. It has been verified that the breakdown voltage of GaN VCD-JBS composed of two cells is 3050 V. Compared with the single cell GaN VCD-JBS, the breakdown voltage is only reduced by 3%, which is negligible. Since each cell shares an identical dielectric layer with an adjacent cell, half of the dielectric layer should be calculated when calculating the on-resistance of the structure.

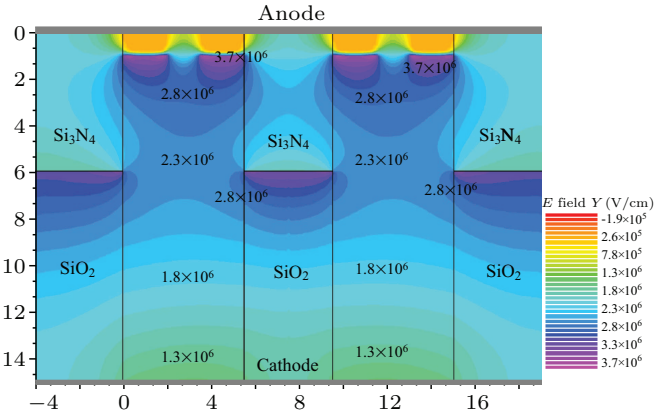


Fig. 9. The distribution of electric field for two cells combination of GaN VCD-JBS.

The above optimization simulations are performed with only one layer of low dielectric constant material. Even if the optimum value is reached, the electric field away from the p–n junction is still low and not uniform enough. In order to make the electric field distributions more uniform and realize a higher breakdown voltage of GaN VCD-JBS, it is necessary to add the multi-layer of the low-K dielectric. The multi-layer of the low-K dielectric can introduce a plurality of electric field peaks to increase the electric field away from the p–n junction surface, resulting in an enhanced BV of the GaN VCD-JBS. Parameters of an optimized structure with three blocks of low-K layers are listed in Table 1.

Table 1. GaN VCD-JBS with three blocks of low-K dielectric layers specifications.

Parameters	Units	Values	Parameter captions
$T_{\text{high }K}$	μm	5	thickness of high K layer
$T_{\text{low }K_1}$	μm	4.5	thickness of low K_1 layer
$T_{\text{low }K_2}$	μm	4.5	thickness of low K_2 layer
$T_{\text{low }K_3}$	μm	1	thickness of low K_3 layer
$L_{\text{h/lcop}}$	μm	4	compound dielectric layers length
N_{pc}	cm^{-3}	1×10^{18}	p-type layer doping concentration
N_{nc}	cm^{-3}	1.5×10^{16}	n-type layer doping concentration
T_{jbs}	μm	15	JBS thickness
L_{jbs}	μm	5.5	length of JBS
L_{p}	μm	2	length of p-type region
T_{p}	μm	1	thickness of p-type region
$L_{\text{p-p}}$	μm	1.5	distance between p-type region
$P_{\text{high }K}$	–	27	relative permittivity of high K layer
$P_{\text{low }K_1}$	–	12	relative permittivity of low K_1 layer
$P_{\text{low }K_2}$	–	7.5	relative permittivity of low K_2 layer
$P_{\text{low }K_3}$	–	3.9	relative permittivity of low K_3 layer

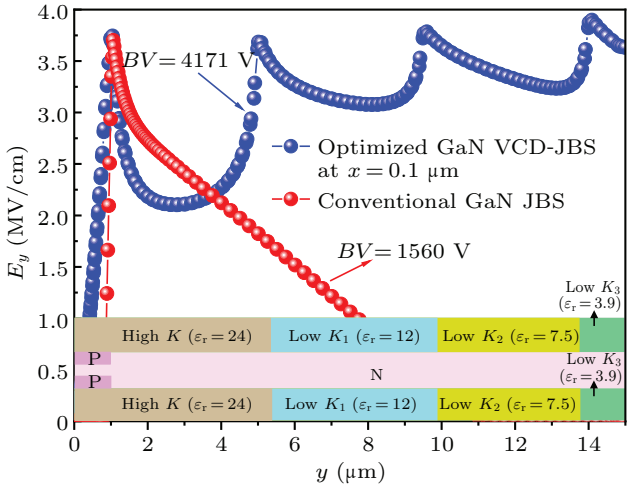


Fig. 10. The electric field distributions corresponding to conventional GaN-based JBS and optimized GaN VCD-JBS at $x = 0.1$ μm.

Figure 10 shows the electric field distribution curve of a conventional JBS and the electric field distribution curve of a GaN VCD-JBS with an optimized multi-layer of the low-K dielectric at $x = 0.1$ μm. Its parameters are shown in Table 1. The concentration of the n-type drift region is 1.5×10^{16} cm^{-3} in the device. The electric field distribution of the optimized GaN VCD-JBS becomes more uniform. The area enclosed by the electric field curve is increased by an enhanced electric field away from the p–n junction. The BV of GaN VCD-JBS reaches 4171 V. Compared with the traditional JBS of $BV = 1560$ V, an increase of 167% is obtained. The forward characteristics of GaN VCD-JBS using multi-layer of low-K dielectric are also excellent. It has a very low on-resistance of 2.07 mΩ·cm^2, and a very high Baliga's figure-of-merit of 8.6 GW/cm^2 is obtained in the optimized GaN VCD-JBS. Therefore, a reasonable optimization of multi-layer of low-K dielectric and high-K dielectric structure can make the electric field distribution more uniform, and thus achieve greater breakdown voltage.

Figure 11 shows the comparison of GaN VCD-JBS in this work with other reported diodes. The high-performance GaN VCD-JBS makes it an advanced high-voltage power device, with the highest BV of 4171 V, an extremely low R_{on} of 2.07 mΩ·cm^2, and an excellent F_{OM} of 8.6 GW/cm^2. The slash lines in Fig. 11 represent the theoretical limits of Si, SiC, and GaN, respectively. The optimized structure is far beyond the theoretical limit of SiC and close to the theoretical limit of GaN. The work represents great potential for GaN VCD-JBS performance.

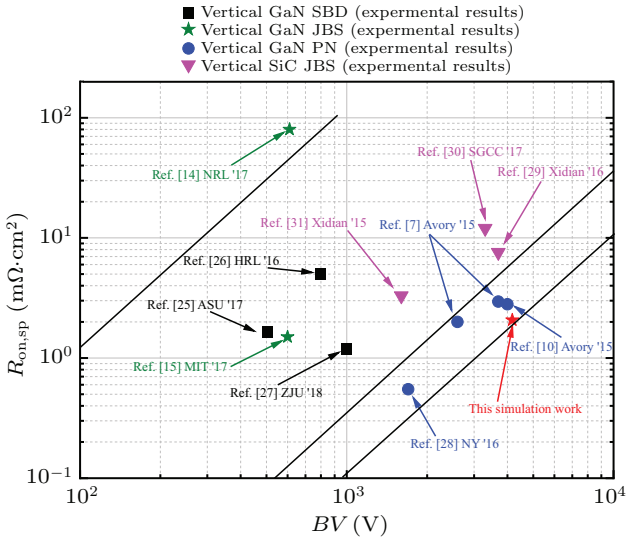


Fig. 11. Baliga's figure-of-merit is shown for state-of-art devices and for our proposed devices from this paper, the 3491 V devices with R_{on} values of 2.2 mΩ·cm^2.

5. Conclusion

In this work, a vertical GaN-based JBS with a high-K/low-K compound dielectric structure (GaN VCD-JBS) is proposed. The electric field peaks introduced by high-K/low-

K dielectric layers make the electric field away from the p–n junction rise and the distribution of the electric field becomes more uniform. The width of Schottky contact W_n, the distance from the interface of p–n junction in JBS to low-K dielectric layer T, and the length of the dielectric layer L of the high K/low K dielectric composite layer are optimized respectively in subsequent work, resulting in superior forward and reverse characteristics. The simulation results show that when the drift region thickness of GaN VCD-JBS is 15 μm and the drift region concentration is 1.5×10^{16} cm^{-3}, a high BV of 4171 V and low $R_{on,sp}$ of 2.07 mΩ·cm^2 for GaN VCD-JBS with three low K dielectric composite layers can be achieved, and the Baliga's figure-of-merit is 8.6 GW/cm^2. This structure shows the potential of GaN JBS as a power diode and provides new ideas for designing high withstand voltage devices.

Acknowledgements

Project supported by the National Natural Science Foundation of China (Grant No. 61376078) and the Natural Science Foundation of Sichuan Province, China (Grant No. 2022NSFSC0515).

References

[1] Millan J, Godignon P, Perpina X, Perez-Tomas A and Rebollo J 2014 *IEEE Trans. Power Electron.* **29** 2155
[2] Kizilyalli I C, Edwards A P, Aktas O, Prunty T and Bour D 2015 *IEEE Trans. Electron. Dev.* **62** 414
[3] Wang Z X, Du L, Liu J W, Wang Y, Jiang Y, Ji S W, Dong S W, Chen W W, Tan X H, Li J L, Li X J, Zhao S L, Zhang J C and Hao Y 2020 *Chin. Phys. B* **29** 027301
[4] Hatakeyama Y, Nomoto K, Terano A, Kaneda N, Tsuchiya T, Mishima T and Nakamura T 2013 *Jpn. J. Appl. Phys.* **52** 028007
[5] Zhang Y H, Yuan M Y, Chowdhury N, Cheng K and Palacios T 2018 *IEEE Electron Dev. Lett.* **39** 715
[6] Chen S H, Chen H, Qiu Y B and Liu C 2021 *IEEE Trans. Electron. Dev.* **68** 5707
[7] Zhang Y H, Piedra D, Sun M, Hennig J, Dadgar A, Yu L and Palacios T 2017 *IEEE Electron Dev. Lett.* **38** 248
[8] Kizilyalli I C, Edwards A P, Nie H, Bour D, Prunty T and Disney D 2014 *IEEE Electron Dev. Lett.* **35** 247
[9] Ohta H, Kaneda N, Horikiri F, Narita Y, Yoshida T, Mishima T and Nakamura T 2015 *IEEE Electron Dev. Lett.* **36** 1180
[10] Bian Z L, Zeng K and Chowdhury S 2022 *IEEE Electron Dev. Lett.* **43** 596
[11] Armstrong A M, Allerman A A, Pickrell G W, Crawford M H, Glaser C E and Smith T 2021 *IEEE J. Electron Dev.* **9** 318
[12] Lee K H, Chang S J, Chang P C, Wang Y C and Kou C H 2008 *Appl. Phys. Lett.* **93** 132110
[13] Jia X Y, Chen S H, Liu Y J, Hou X, Zhang Y H, Zhang Z H and Kou H C 2020 *IEEE Trans. Electron. Dev.* **67** 1931
[14] Zhou F, Xu W Z, Ren F F, Zhou D, Chen D J, Zhang R, Zheng Y D, Zhu T G and Lu H 2021 *IEEE Electron Dev. Lett.* **42** 974
[15] Zhang Y H, Liu Z H, Tadjer M J, Sun M, Piedra D, Hatem C, Anderson T J, Luna L E, Nath A, Koehler A D, Okumura H, Hu J, Zhang X, Gao X, Feigelson B N, Hobart K D and Palacios T 2017 *IEEE Electron Dev. Lett.* **38** 1097
[16] Hanawa H, Onodera H, Nakajima A and Horio K 2014 *IEEE Trans. Electron. Dev.* **61** 769
[17] Liu C, Chor E F and Tan L S 2007 *Semicond. Sci. Technol.* **22** 522
[18] Kabemura T, Ueda S, Kawada Y and Horio K 2018 *IEEE Trans. Electron. Dev.* **65** 3848
[19] Du J F, Li Z C, Liu D, Bai Z Y, Liu Y and Yu Q 2017 *Superlattice. Microst.* **111** 302
[20] Pipinys P and Lapeika V 2006 *J. Appl. Phys.* **99** 093709
[21] Albrecht J D, Wang R P, Ruden P P, Farahmand M and Brennan K F 1998 *J. Appl. Phys.* **83** 4777
[22] Farahmand M, Garetto C, Bellotti E, Brennan K F, Goano M, Ghillino E, Ghione G, Albrecht J D and Ruden P P 2001 *IEEE Trans. Electron. Dev.* **48** 535
[23] Oguzman I H, Bellotti E, Brennan K F, Kolnik J, Wang R P and Ruden P P 1997 *J. Appl. Phys.* **81** 7827
[24] Farzana E, Wang J F, Monavarian M, Itoh T, Qwah K S, Biegler Z J, Jorgensen K F and Speck J S 2020 *IEEE Electron Dev. Lett.* **41** 1806
[25] Fu H Q, Huang X Q, Chen H, Lu Z J, Baranowski I and Zhao Y J 2017 *Appl. Phys. Lett.* **111** 152102
[26] Cao Y, Chu R, Li R, Chen M, Chang R and Hughes B 2016 *Appl. Phys. Lett.* **108** 062103
[27] Han S W, Yang S and Sheng K 2018 *IEEE Electron Dev. Lett.* **39** 572
[28] Nomoto K, Song B, Hu Z Y, Zhu M D, Qi M, Kaneda N, Mishima T, Nakamura T, Jena D and Xing H G 2016 *IEEE Electron Dev. Lett.* **37** 161
[29] Yuan H, Song Q W, Tang X Y, Zhang Y M, Zhang Y M and Zhang Y M 2016 *Solid State Electron.* **123** 58
[30] Pan Y, Tian L, Wu H, Li Y P and Yang F 2017 *Microelectron. Eng.* **181** 10
[31] Song Q W, Yuan H, Han C, Zhang Y M, Tang X Y, Zhang Y M, Guo H, Zhang Y M, Jia R X and Wang Y H 2015 *Sci. China Technol. Sci.* **58** 1369